HHS Public Access

Retinal origin of orientation maps in visual cortex

Se-Bum Paik[1] and **Dario L. Ringach**[1,2]

[1]Department of Neurobiology, David Geffen School of Medicine, University of California Los Angeles, Los Angeles, California, USA

[2]Department of Psychology, University of California, Los Angeles, CA 90095

Abstract

The orientation map is a hallmark of primary visual cortex in higher mammals. It is not yet known how orientation maps develop, what function they play in visual processing and why some species lack them. Here we advance the notion that quasi-periodic orientation maps are established by moiré interference of regularly spaced ON and OFF-center retinal ganglion cell mosaics. A key prediction of the theory is that the centers of iso-orientation domains must be arranged in a hexagonal lattice on the cortical surface. Here we show that such pattern is observed in individuals of four different species: monkey, cat, tree shrew and ferret. The proposed mechanism explains how orientation maps can develop without requiring precise patterns of spontaneous activity or molecular guidance. Further, it offers a possible account for the emergence of orientation tuning in single neurons despite the absence of orderly orientation maps in rodents species.

It has long been known that the primary visual cortex of higher mammals is organized into functional maps[1]. One of the most studied is the orientation map, which captures the preferred orientation of neurons across the cortical surface. Optical imaging methods[2–3] have revealed that preferred orientation on the cortex changes continuously in a quasi-periodic fashion, except at intermittent point discontinuities (pinwheels) and line discontinuities (fractures) where orientation preference jumps in a seemingly rapid way[4–6]. Although much effort has been devoted to the study of cortical maps, we still lack a full account of how they develop and what function they play in normal visual processing[7–9].

The quasi-periodicity of cortical maps has been postulated to establish sensory modules that serve to process signals from a single location on the visual field by a heterogeneous set of receptive fields[8]. However, it is now recognized that some species lack orientation maps despite having simple-cells exhibiting normal receptive field structure and orientation selectivity[10–11]. Similarly, the expression of ocular dominance columns varies widely across individual members of a species[12], and is entirely absent in some species that, nevertheless, show normal evoked potentials to stereoscopic stimuli[13]. Such findings raise doubts about the functional significance of cortical maps in visual processing.

Important clues regarding the wiring of orientation maps and receptive fields of neurons are found in early development. In kittens, orientation-tuned responses can be measured as soon as they open their eyes about a week after birth[14]. Orientation columns (the clustering of cells with similar preferences) and maps are also present at this early stage. This organization is established without exposure to normal visual experience[14–17], which is otherwise needed for receptive fields and maps to reach full maturation[15, 18].

The development of the spatial structure of cortical receptive fields also offers important hints. A key observation is that simple-cell receptive fields appear to develop *without* an intermediate phase of segregation between ON and OFF sub-regions[19–20] (as assumed by dominant developmental models[21–23]). This is surprising because the classical view holds that numerous geniculate afferents, with overlapping ON- and OFF-center receptive fields, must be sorted out by cortical neurons to generate simple cells with segregated ON- and OFF- subregions[24]. And yet, this segregation process has never been observed experimentally. Instead, the available data in cat indicate the ratio of simple-cells (having one or more segregated sub-regions) to complex-cells (having overlapping ON/OFF responses) remains approximately constant during development[19–20]. This suggests cortical cells have a normal receptive field organization as soon as it is possible to record visually evoked responses from them[14, 20, 25].

How can receptive fields and maps be wired so early in development? Our study builds upon the statistical connectivity hypothesis which provides some initial answers to this question[26–27]. The basic idea is that receptive fields and orientation maps in the cortex are constrained by the spatial distribution of ON- and OFF-center receptive fields in retinal mosaics[26], a notion that goes back to pioneering work by Wässle and collaborators[28] and Soodak[29]. These constraints seed the structure of receptive fields and maps in the cortex upon which other developmental processes, such as activity-dependent refinement and maintenance, act during the critical period.

The present work advances the theory by answering an important question: how does the model generate *periodic* orientation maps? Here we show that periodicity of the map can arise from the moiré interference pattern of retina ganglion cells (RGC) mosaics which is mirrored in the lateral geniculate nucleus (LGN) and generates a quasi-periodic input into the cortex. As we will see, this insight provides a simple explanation for the generation of simple-cell receptive fields and orientation maps, making novel predictions about their organization.

A central prediction of the model is that iso-orientation domains should lie on a hexagonal lattice on the cortical surface. Here we show that this arrangement is observed in all four different species examined so far: monkey, cat, ferret and tree shrew, providing experimental support for the model. Moreover, our analyses demonstrate the model admits regimes where orientation tuning in individual cells can arise *without* the emergence of an orderly orientation map, potentially extending the theory to incorporate rodent species.

Results

Orientation maps as moiré interference of RGC mosaics

We propose that the cortical orientation map is seeded by moiré interference[30] between ON- and OFF-center receptive fields of one type of ganglion cell in the retina. We introduce our model by considering an ideal case where the locations of ON- and OFF-center receptive fields lie at the vertices of perfect hexagonal lattices. This is a sensible starting point because it is known that their local structure is a noisy hexagonal lattice[28], as inferred from the fact that the angle formed by a cell body with its neighbors of the same sign has modes at multiples of 60 deg (see Supplementary Fig 1 for another demonstration). The ON and OFF lattices are also known to be independent from each other in the sense that knowledge of the location of a cell from one sign does not provide information as to the location of cells of the other[31–32]. When two hexagonal lattices are superimposed in such a fashion the result is a periodic interference pattern (Fig. 1a). An important property of the resulting pattern is that the nearest neighbor of an ON-center cell is an OFF-center cell (and vice-versa), a feature that is also observed in the statistics of RGC mosaics reconstructed experimentally[28, 33] (Fig. 1b, see also Fig. 4a). We call such a pair of opposite-sign, nearest neighbors a *dipole* and assign to it an orientation that is perpendicular to the line joining the centers of the constituent receptive fields (Fig. 1b).

The statistical wiring model posits that pooling inputs of nearby RGC receptive fields (relayed by cells in the LGN[34]), using an isotropic weighting function, is sufficient to generate orientation tuning and simple-cell receptive field structure[26–27]. If the input to a cortical cell is dominated by a single RGC dipole then the resulting receptive field will have a structure similar to that of a simple-cell, with side-by-side sub-regions of opposite sign, and its preferred orientation will match that of the dipole (Fig. 1b). The receptive fields generated by the model are *not* always dominated by single dipoles[26], but those satisfying this condition tend to be the ones that are most sharply tuned for orientation (Fig. 1d). Thus, the orientation of RGC dipoles provides a good approximation to the structure of the orientation map seeded by the model. This simplification allows us to derive and understand many important properties of the cortical map predicted by the theory in a rather simple and intuitive manner.

Periodicity of the orientation map

From the preceding discussion it is clear that the period of the orientation map is determined by the period of the moiré pattern itself, d_M (Fig 1a), which is given by[35]

$$d_M = \left(\frac{1+\alpha}{\sqrt{\alpha^2 + 2(1-\cos\theta)(1+\alpha)}} \right) d \equiv S \times d \quad (1)$$

Here, d represents the spacing of the first lattice, $(1+\alpha)d$ is the spacing of the second lattice, and θ their relative orientation. We define the *scaling factor* as the ratio between the period of the interference pattern and that of the lattice, $S \equiv d_M / d$ (Fig. 1c). This ratio is important because it determines how many RGC receptive fields are involved in the construction of one cortical hyper-column.

The parameters (α, θ) determine the scaling factor and the operating regime of the model. Operating regimes that yield small values of the scaling factor (less than ~3) generate a salt-and-pepper like organization because the period of the interference pattern becomes comparable to the distance between the centers of nearest-neighbors receptive fields in the mosaics (Fig 2, right column). Operating regimes with scaling factors between 4–16 generate interference patterns that, once the cortical magnification factor is taken into account (cf. calculation in Supplementary Information), can match the periodicity of experimentally measured maps in primates (Fig 2, middle column). Regimes near the origin $(\alpha,\theta)=(0,0)$ generate large scaling factors and, as a consequence, preferred orientation changes very slowly across cortical space (Fig 2, left column).

Orientation maps have hexagonal symmetry

One surprising prediction can be derived from the ideal model by examining the structure of the moiré interference patterns. Each pattern is periodic, with all possible orientations appearing within one cycle, changing smoothly across cortical space (Fig 1a,d). The hexagonal symmetry of the interference pattern predicts that (assuming an isotropic magnification factor) locations with the same orientation preference should be arranged in a hexagonal lattice pattern as well (Fig 1d, 2c).

We tested this prediction using published orientation maps from different species. In each case, we begin by representing each map as a two-dimensional image $\theta(x,y)$ and compute a two-dimensional (circular) auto-correlation as follows:

$$r\left(\Delta x, \Delta y\right) = \frac{1}{N}\sum_{x,y}\left(\left|\exp\left(2i\theta\left(x,y\right)\right) + \exp\left(2i\theta\left(x+\Delta x, y+\Delta y\right)\right)\right| - 1\right)$$

In other words, two copies of the same map are shifted relative to each other by (x, y) and the agreement between the orientations in the shifted maps are assessed in the region of overlap by an averaged vector resultant (the region of overlap has N pixels). If all the values between two maps in overlapped areas match closely we obtain a value $r \approx 1$. If the orientations at each location between two maps are orthogonal, $r = -1$.

The auto-correlation functions, evaluated in two individuals of four different species, show a pattern of discrete, secondary peaks around the origin that resemble a hexagon (Fig 3a) (see also Supplementary Fig 2). In each case, the auto-correlation functions are scaled and rotated to map the local peak with the largest magnitude onto the point (0,1) in the plane. The statistical significance of the local peaks is assessed by generating control maps with an isotropic amplitude spectrum matching that of experimental maps and computing the distribution of amplitudes of secondary peaks from such a family of control maps (calculation detailed in Supplementary Fig 3). All the secondary peaks shown in the figure (solid dots in Fig 3a) attain a significance level of $p < 0.002$. In other words, the local peaks are very unlikely to have been generated by chance assuming the null hypothesis that orientation maps are isotropic.

Next, we computed the average auto-correlation function across individuals and species (Fig 3b). The result shows local peaks (Fig 3b, open white squares) that very closely match the hexagonal prediction (Fig 3b, open white circles). The distribution of local maxima in the individual cases (Fig 3a, black solids dots), superimposed on top of the mean auto-correlation function, cluster around the vertices of the hexagon (Fig 3b, black solid dots). This observation can be validated by the distribution of the angular location of the peaks relative to the reference point at (0,1), which is clearly bimodal (Fig 3c). When we fit the angular distribution with a mixture of von Mises components we find the data are best explained by a mixture of two components (Fig 3c, red solid line, model selection by Bayesian information criterion). The modes of the components match very well their predicted location at 60 and 120 deg. Thus, the angular distribution of local maxima is consistent with that of a hexagonal lattice. When the same analysis is repeated on the control maps we find that the magnitudes of the local peaks are substantially smaller (as already reflected in the fact that only 1 in 500 control maps attained peaks of similar magnitude by chance). Furthermore, the angular distribution of local peaks whose magnitudes reach statistical significance by chance is rather uniform, with a depletion of points near the reference point that results from the alignment procedure (Fig 3d,e). Finally, for comparison, we performed the same analysis on orientation maps generated by an activity dependent model[36]. We find this model does not generate auto-correlations with any secondary peaks of statistically significant magnitude (data not shown).

Effects of RGC lattice noise on map periodicity

Of course, RGC mosaics are not perfect hexagonal lattices. This raises the question of whether the proposed mechanism is capable of seeding an orientation map after the addition of realistic levels of noise in the positions of the RGC receptive fields. We tested this by perturbing the vertices of the hexagonal lattices with independent two-dimensional Gaussian noise to match the nearest-neighbor statistics in experimentally measured mosaics[26]. A ratio between the standard deviation and the average of the lattice spacing equal to $\sigma / d \simeq 0.12$ provides a very good match to the distributions of nearest-neighbour receptive fields in the experimental data (Fig 4a). We found that even with such realistic level of noise the interference pattern remains strong enough to generate a periodic orientation map (Fig 4b,c). The periodicity of the map can be evaluated by measuring the amplitude and location of the secondary peaks in the auto-correlation of the simulated orientation map as a function of noise level (Fig 4b). The normalized period of the map (relative to the ideal case) remains very stable (Fig 4b, right panel) and the magnitude of the secondary peak is positive and substantially larger than zero (Fig 4b, middle panel), indicating a robust periodic structure.

Insight into the robustness of the seeded map is gained by calculating the number of original dipoles in the interference pattern that are lost as positional noise increases (Fig 4c) and, of those that remain, how much their orientation is perturbed relative to that of their original configuration (Fig 4d). We recall a dipole was defined by two cells of opposite sign that are nearest neighbours of each other. As the positional noise increases, the conditions defining a given dipole may cease to hold, in which case we say the dipole is *lost*. Simulations show a roughly linear increase in the fraction of dipoles lost with increasing levels of noise, reaching a value of 27% for realistic levels. Thus, about 73% of the dipoles of the original

pattern survive. Of those dipoles remaining, their orientation is still close to that of their original configuration (Fig 4d). These data clarify the reasons behind the robustness of the seeded map to positional noise. An example of an interference pattern with realistic noise levels and the resulting orientation map is provided in Supplementary Fig 4.

Robustness of receptive field structure to positional noise

What is the spatial structure of simple-cell receptive fields generated by the model and how are they affected by the presence of positional noise? To answer this question, we fitted a two-dimensional Gabor function to the simulated simple-cell receptive fields at randomly chosen cortical sites. The Gabor function was defined by[37]:

$$h(x,'y') = A \exp\left(-\left(x'/\sqrt{2}\sigma_{x'}\right)^2 - \left(y'/\sqrt{2}\sigma_{y'}\right)^2\right) \cos\left(2\pi f x' + \phi\right)$$

where the coordinate system (x', y') is obtained by translating the original by $x_0, y_0)$ and rotating it by γ.

$$x' = (x - x_0)\cos\gamma + (y - y_0)\sin\gamma$$
$$y' = -(x - x_0)\sin\gamma + (y - y_0)\cos\gamma$$

In the (x',y') plane, the modulation of the sinusoidal function is along the x' axis, while $\sigma_{x'}$ and $\sigma_{y'}$ represent the width of the Gaussian envelope along each axis respectively. The spatial phase is determined by φ, which leads to even-symmetric profiles for $\varphi = 0$ and odd-symmetric for $\varphi = \pi / 2$.

We analyzed the data by looking at the distribution of $n_{x'} = \sigma_x f$ and $n_{y'} = \sigma_y f$, as previously done in the experimental study of primate data[37]. These numbers can be thought as a measure of the width of the Gaussian envelope along each axis in units of the period of the underlying sinusoidal grating.

We find that the distribution of $n_{x'}$ and $n_{y'}$ remains largely unaffected by changes in scaling factor and level of RGC lattice noise (Fig. 5). The reason for this is that the local structure of receptive fields is solely dependent on the statistics of nearest-neighbor distributions (Fig 4a). So long as there is high probability that the nearest neighbor of one cell is one the opposite sign, the model will generate dipoles can induce similar families of simple-cell RFs. The theory thus admits a regime where single neurons can be well-tuned for orientation despite the absence of a smooth orientation map, as is observed in rodents (Fig 2, right column).

The distribution of spatial phases of the predicted receptive fields is also of interest (Fig 5, inset histograms). The simulations indicate that odd-symmetric receptive fields tend to be well-tuned for orientation. This is due to the fact that inputs to a cell dominated by a single dipole will generate a well-tuned, odd-symmetric receptive field. Even-symmetric receptive fields can be either broadly tuned (with one effective sub-region), or sharply tuned (with three effective sub-regions of alternating signs). The tendency for well-tuned cells in the

model to shift their spatial-phase towards odd-symmetry is consistent with experimental observation[37].

Discussion

Where do orientation maps come from? Here we put forward the notion that periodic orientation maps arise from the moiré interference pattern of quasi-regular retinal mosaics (Fig 1). A central prediction of the model is that iso-orientation domains should be arranged approximately in a hexagonal lattice on the cortical surface. Indeed, we found this property in all four different species tested: ferrets, tree shrews, cats and monkeys. Such a novel, universal property of maps provides support for the model.

Several puzzling findings of visual development are parsimoniously explained by the model. Moiré interference explains how cortical receptive fields and maps may arise even in the absence of precisely structured activity in the developing thalamus[22, 36, 38]. This is because RGC mosaics themselves can develop without the need for visual experience[39]. The theory solves the dilemma of how simple cells can arise in early development without an intermediate phase of segregation between ON- and OFF-center inputs[19–20]. It further accounts for a segregation of ON- and OFF-center afferents into cortical domains[40]. Both results are a consequence of the limited overlap between nearest neighbors in retinal mosaics.

The emergence of orientation columns is also explained by the model, as in this scenario cortical neurons in a column receive inputs from the same set of RGCs and thus their receptive fields are constrained in the same way. If the input determines the preferred orientation of the cortical column then the emergence of orientation columns is easily understood. Experimental confirmation of this idea is provided by the recent finding that the distribution of ON- and OFF-center receptive fields in the LGN predicts the orientation preference of its target cortical column[41]. This result is remarkable because it implies that the orientation map is already coded in the LGN. Competing theories based on activity-dependent wiring do not account for the orientation bias present in the LGN input and how it can successfully predict the preferred orientation of their cortical targets.

During development a diverse set of receptive fields is observed in the thalamus, some of which show ON and OFF sub-regions and orientation tuning[42]. Such intermediate stage is consistent with our model in that, before the pruning of retino-geniculate inputs, thalamic cells may pool from more than one RGC mosaic resulting in receptive fields similar to those generated by the model. Tavazoie and Reid postulated that this intermediate stage, along with activity-dependent learning, could generate orientation tuned cells in the cortex. We note that unless one also incorporates the key constraints established by the retinal input, such a mechanism alone fails to account for the emergence of orientation columns.

The simultaneous mapping of simple-cell receptive fields in a population of nearby cortical cells can also serve to test our hypothesis that RFs are constructed from a limited number of inputs. For example, a recent two-photon imaging of mouse visual cortex reveals that nearby

simple-cell receptive fields often share common sub-regions with the same location and shape[43], consistent with the notion they are all constructed from a limited input[26].

The model admits a regime where single cells are well tuned despite the absence of an orientation map. This was demonstrated by the invariance of the receptive field structure (documented by the distribution of (n_x,n_y) values) with changes in the scaling factor and positional noise (Fig 5). The theory thus offers a potential explanation for how the properties of simple-cell receptive fields could be similar in mouse, cat and monkey[37, 44]. We must exercise caution as a small scaling factor is only one possible explanation of this phenomenon. In general, if the emergence of the moiré interference pattern is disrupted for any reason, it will lead to a failure in the creation of orientation maps. To some extent this situation may already arise at the fovea, where dedicated one-to-one lines for ON- and OFF-center receptive fields increase their overlap compared to those in parafovea. Indeed, near the fovea the orientation map appears disrupted in double-label 2DG studies[45], which is also consistent with the fact that orientation-tuned neurons near the fovea are less numerous and more broadly tuned than those in the parafovea[46].

The present scope of the model is limited to explaining how the inputs from the contra-lateral eye, which invade the cortex ahead of those from the ipsilateral eye, could establish an initial blueprint for receptive field and maps. The orientation map is expected to change as input from the ipsilateral eye is accommodated and both orientation maps come into register, but not so much as to erase all vestiges of the initial map organization[15]. Even during this process the geniculate inputs will continue to constrain the range of preferred orientations attainable at any cortical site from any given eye. In other words, these constraints ought to be taken into account in models that study activity-dependent matching of the orientation maps of the two eyes.

Finally, the theory predicts the existence of what might call orientation scotomas: at some locations, the cortex cannot represent every orientation equally well. This results from the fact that limited retinal resources at some locations prohibit the implementation of receptive fields with a complete set of preferred orientations (Fig 1d, shaded areas). We are now testing this prediction by mapping human orientation discrimination thresholds of very small stimuli in the far periphery. A confirmation of orientation scotomas would provide further support for the theory and invalidate our present view of the cortex as analyzing the local image by a homogeneous set of filters tuned to different orientations. Although controversial, we note that a previous study[47] found that pairs of cells in the cortex must have their receptive field centers one diameter apart to ensure their orientation preferences are, on average, orthogonal to one another, a finding consistent with the notion of orientation scotomas.

To summarize, moiré interference offers a novel mechanism for the *initial seeding* of a periodic orientation map and simple-cell receptive fields that does not require specific patterns of spontaneous thalamic activity, the presence of molecular markers or cortical scaffolding. The simplicity of the model, the parsimonious explanations it offers to several key findings, and the recent confirmation of several of its predictions are all encouraging. The hexagonal structure in the auto-correlation of orientation maps of various species now

provides additional support for our hypothesis which awaits its ultimate test -- an experiment that can reveal a correlation between the structure of the RGC mosaics and the orientation maps measured in the same individuals.

Methods

The simulations were performed using the statistical wiring model published earlier. We briefly summarize the algorithm here and refer the reader to the justification for the selection of parameters to our earlier work[26–27].

Structure of retinal ganglion cell mosaics

Simulated RGC mosaics were generated by adding various amount of random displacement to each vertex of a hexagonal lattice that represents the position of ON- and OFF-center receptive fields[26].

The centers of RGC receptive field position vectors are defined by

$$r_{OFF}=d_{OFF}L+\eta$$
$$r_{ON}=d_{ON}R_\theta L+\eta+\eta_0$$

where perfect hexagonal grids

$$L=\frac{1}{2}\left[\begin{array}{cc} 1 & 1 \\ \sqrt{3} & -\sqrt{3} \end{array}\right]\left[\begin{array}{c} i \\ j \end{array}\right] \quad i,j=0,\pm1,\pm2,\cdots$$

are first scaled by the desired grid spacing, d_{OFF} and $d_{ON} = d_{OFF}(1+\alpha)$. The ON-center cell lattice is then rotated relative to the OFF-center cell lattice by a matrix

$$R_\theta=\left[\begin{array}{cc} \cos\theta & \sin\theta \\ -\sin\theta & \cos\theta \end{array}\right]$$

Then the cell position vectors are perturbed by the addition of i.i.d. positional noise described by η. The standard deviation of the noise, σ, is conveniently expressed as a fraction of the grid spacing, d_{OFF}. The noise-free ideal model corresponds to $\sigma = 0$. A random relative spatial shift between the two mosaics η_0 can be added. However, except for the particular case where $\alpha = 0$ this has no consequence for the results because a rotation and translation can be written as a rotation around a different center.

To calculate nearest neighbor statistics in experimental mosaics we used digitized maps of receptive field reconstructions from the macaque monkey retina, published by Gauthier et al. (2009), modeling the center of the receptive fields as a two-dimensional Gaussian with a standard deviation of 60μm in retinal space.

Statistical connectivity and receptive field computation

The statistical wiring model includes a stochastic component that allows cells in the same cortical column to develop slightly different receptive fields, because both the probability of connection and its strength are random variables[26]. In this work, we did not simulate the whole model but only computed the mean receptive field at each location. We have previously shown the mean receptive field can be computed as a weighted sum of the

afferent LGN input: $\Psi = \sum_i \exp\left(-\left(d_i^2/2\overline{\sigma}^2\right)\right) \cdot \Psi_i^{LGN}$ where $\overline{\sigma} = \frac{\sigma_{conn} \cdot \sigma_{syn}}{\sqrt{\sigma_{conn}^2 + \sigma_{syn}^2}} \Psi_i^{LGN}$ is

the receptive field of the i-th LGN neuron, d_i is the distance between the locations of the LGN afferent and the cortical site where we are calculating the mean receptive field. The values of σ_{conn} and σ_{syn} were set as 25μm of cortical space and they represent the rate of the spatial fall-out of the probability of connectivity and synaptic strength respectively, which are assumed to be Gaussian. (cf. ref[27] for a detailed description of these parameters and derivations).

Cortical map measurements

Once the mean receptive field was calculated at each cortical position we estimated its preferred orientation and selectivity from its Fourier transform $\Psi(\omega)$ as follows. The preferred orientation is defined as $\theta_{pref} = \arg(\mu)/2$, where

$$\mu = \int |\Psi(\omega)| \, |\omega| \exp\left(2i \arg(\omega)\right) d\omega / \int |\Psi(\omega)| d\omega.$$

Orientation selectivity index (OSI) was defined as

$$OSI = \frac{\left| \int |\Psi(\omega_{pref}, \theta)| \exp(2i\theta) d\theta \right|}{\int |\Psi(\omega_{pref}, \theta)| d\theta}$$

where $\omega_{pref} = |\mu|$ is the preferred spatial frequency of the receptive field filter.

Selectivity-weighted orientation map

The predicted orientation selectivity index (OSI) varies across the cortex and it is maximal at locations where cortical sites receive input dominated from a single dipole. These strongly tuned sites contribute largely to the orientation tuning in the cortex, thus seeding the orientation map. To identify the location and preferred orientation angles of such signals we sample the cortical locations with OSI higher than a specified threshold of OSI>0.25 (Fig 1d, 2d, and Supplementary Fig 4). For visualization, a smooth continuous version of the map is then obtained by diffusion of orientations with a Gaussian window of 140um in cortical space. The smooth representation of these maps are shown in the right panels of Fig 1d, 2b and Supplementary Fig 4.

Analysis of experimental orientation maps

Regions of interest (ROI) in the experimental maps were selected by avoiding areas that were too close to the V1/V2 boundary and having an intermediate size (~3×3 orientation

periods). For each individual we choose between 2 to 4 non-overlapping ROIs. Selecting ROIs of intermediate size is important because locally the maps can have hexagonal structure, but over a long range the orientation of the structure can drift. In such a case, computing the auto-correlation of over a very large area can obliterate the secondary peaks observed in the auto-correlation function using smaller ROIs. On the other hand, the smaller the ROI the more likely we are to obtain peaks in the auto-correlation by mere chance. Thus, we adopted a strategy where we averaged the auto-correlation functions of non-overlapping ROIs for each individual after appropriate normalization (see Supplementary Fig 2).

To compute the statistical significance of secondary peaks in the auto-correlation function we calculated the probability that they could have resulted by chance from control orientation maps. These control maps were generated by enforcing their Fourier amplitude spectrum to be isotropic and having the same marginal, radial amplitude spectrum, of the map under consideration (a detailed description of the method is provided in the Supplementary Information and Supplementary Fig 3).

Orientation maps from cat visual cortex were shared by Dr. Matteo Carandini and colleagues, while tree shrew and ferret data were provided by Dr. David Fitzpatrick and colleagues. Orientation maps from primary visual cortex were obtained from ref[48].

Supplementary Material

Refer to Web version on PubMed Central for supplementary material.

Acknowledgements

References

1. Hubel DH, Wiesel TN. Ferrier lecture. Functional architecture of macaque monkey visual cortex. Proc R Soc Lond B Biol Sci. 1977; 198:1–59. [PubMed: 20635]

2. Blasdel GG, Salama G. Voltage-Sensitive Dyes Reveal a Modular Organization in Monkey Striate Cortex. Nature. 1986; 321:579–585. [PubMed: 3713842]

3. Ts'o DY, Frostig RD, Lieke EE, Grinvald A. Functional organization of primate visual cortex revealed by high resolution optical imaging. Science. 1990; 249:417–420. [PubMed: 2165630]

4. Obermayer K, Blasdel GG. Geometry of Orientation and Ocular Dominance Columns in Monkey Striate Cortex. Journal of Neuroscience. 1993; 13:4114–4129. [PubMed: 8410181]

5. Bonhoeffer T, Grinvald A. The Layout of Iso-Orientation Domains in Area-18 of Cat Visual-Cortex - Optical Imaging Reveals a Pinwheel-Like Organization. Journal of Neuroscience. 1993; 13:4157–4180. [PubMed: 8410182]

6. Bonhoeffer T, Grinvald A. Iso-Orientation Domains in Cat Visual-Cortex Are Arranged in Pinwheel-Like Patterns. Nature. 1991; 353:429–431. [PubMed: 1896085]

7. Purves D, Riddle DR, Lamantia AS. Iterated Patterns of Brain Circuitry (or How the Cortex Gets Its Spots). Trends in Neurosciences. 1992; 15:362–368. [PubMed: 1279855]

8. Horton JC, Adams DL. The cortical column: a structure without a function. Philosophical Transactions of the Royal Society B-Biological Sciences. 2005; 360:837–862.

9. Van Hooser SD. Similarity and diversity in visual cortex: is there a unifying theory of cortical computation? Neuroscientist. 2007; 13:639–656. [PubMed: 17911223]

10. Ohki K, Chung S, Ch'ng YH, Kara P, Reid RC. Functional imaging with cellular resolution reveals precise micro-architecture in visual cortex. Nature. 2005; 433:597–603. [PubMed: 15660108]

11. Van Hooser SD, Heimel JAF, Chung S, Nelson SB, Toth LJ. Orientation selectivity without orientation maps in visual cortex of a highly visual mammal. Journal of Neuroscience. 2005; 25:19–28. [PubMed: 15634763]

12. Adams DL, Horton JC. Capricious expression of cortical columns in the primate brain. Nature Neuroscience. 2003; 6:113–114. [PubMed: 12536211]

13. Livingstone MS, Nori S, Freeman DC, Hubel DH. Stereopsis and Binocularity in the Squirrel-Monkey. Vision Research. 1995; 35:345–354. [PubMed: 7892730]

14. Hubel DH, Wiesel TN. Receptive Fields of Cells in Striate Cortex of Very Young, Visually Inexperienced Kittens. Journal of Neurophysiology. 1963; 26:994. [PubMed: 14084171]

15. Crair MC, Gillespie DC, Stryker MP. The role of visual experience in the development of columns in cat visual cortex. Science. 1998; 279:566–570. [PubMed: 9438851]

16. Chapman B, Stryker MP, Bonhoeffer T. Development of orientation preference maps in ferret primary visual cortex. Journal of Neuroscience. 1996; 16:6443–6453. [PubMed: 8815923]

17. Godecke I, Kim DS, Bonhoeffer T, Singer W. Development of orientation preference maps in area 18 of kitten visual cortex. European Journal of Neuroscience. 1997; 9:1754–1762. [PubMed: 9283830]

18. White LE, Coppola DM, Fitzpatrick D. The contribution of sensory experience to the maturation of orientation selectivity in ferret visual cortex. Nature. 2001; 411:1049–1052. [PubMed: 11429605]

19. Albus K, Wolf W. Early Post-Natal Development of Neuronal Function in the Kittens Visual-Cortex - a Laminar Analysis. Journal of Physiology-London. 1984; 348:153–185.

20. Braastad BO, Heggelund P. Development of spatial receptive-field organization and orientation selectivity in kitten striate cortex. J Neurophysiol. 1985; 53:1158–1178. [PubMed: 3998804]

21. Miller KD. Development of Orientation Columns Via Competition between on-Center and Off-Center Inputs. Neuroreport. 1992; 3:73–76. [PubMed: 1611038]

22. Ohshiro T, Weliky M. Simple fall-off pattern of correlated neural activity in the developing lateral geniculate nucleus. Nat Neurosci. 2006; 9:1541–1548. [PubMed: 17115045]

23. Swindale NV. The development of topography in the visual cortex: A review of models. Network-Computation in Neural Systems. 1996; 7:161–247.

24. Reid RC, Alonso JM. Specificity of Monosynaptic Connections from Thalamus to Visual-Cortex. Nature. 1995; 378:281–284. [PubMed: 7477347]

25. Sherk H, Stryker MP. Quantitative Study of Cortical Orientation Selectivity in Visually Inexperienced Kitten. Journal of Neurophysiology. 1976; 39:63–70. [PubMed: 1249604]

26. Ringach DL. Haphazard wiring of simple receptive fields and orientation columns in visual cortex. Journal of Neurophysiology. 2004; 92:468–476. [PubMed: 14999045]

27. Ringach DL. On the origin of the functional architecture of the cortex. PLoS ONE. 2007; 2:e251. [PubMed: 17330140]

28. Wassle H, Boycott BB, Illing RB. Morphology and Mosaic of on-Beta and Off-Beta Cells in the Cat Retina and Some Functional Considerations. Proceedings of the Royal Society of London Series B-Biological Sciences. 1981; 212:177.

29. Soodak RE. The Retinal Ganglion-Cell Mosaic Defines Orientation Columns in Striate Cortex. Proceedings of the National Academy of Sciences of the United States of America. 1987; 84:3936–3940. [PubMed: 3108884]

30. Amidror, I. The theory of the Moiré phenomenon. Norwell, Massachusetts: Kluwer Academic; 2000.

31. Rockhill RL, Euler T, Masland RH. Spatial order within but not between types of retinal neurons. Proc Natl Acad Sci U S A. 2000; 97:2303–2307. [PubMed: 10688875]

32. Eglen SJ, Diggle PJ, Troy JB. Homotypic constraints dominate positioning of on- and off-center beta retinal ganglion cells. Visual Neuroscience. 2005; 22:859–871. [PubMed: 16469193]

33. Gauthier JL, et al. Uniform signal redundancy of parasol and midget ganglion cells in primate retina. J Neurosci. 2009; 29:4675–4680. [PubMed: 19357292]

34. Usrey WM, Reppas JB, Reid RC. Specificity and strength of retinogeniculate connections. Journal of Neurophysiology. 1999; 82:3527–3540. [PubMed: 10601479]

35. Blair HT, Welday AC, Zhang K. Scale-invariant memory representations emerge from moire interference between grid fields that produce theta oscillations: a computational model. J Neurosci. 2007; 27:3211–3229. [PubMed: 17376982]

36. Miller KD. A Model for the Development of Simple Cell Receptive-Fields and the Ordered Arrangement of Orientation Columns through Activity-Dependent Competition between on- and Off-Center Inputs. Journal of Neuroscience. 1994; 14:409–441. [PubMed: 8283248]

37. Ringach DL. Spatial structure and symmetry of simple-cell receptive fields in macaque primary visual cortex. Journal of Neurophysiology. 2002; 88:455–463. [PubMed: 12091567]

38. Miller KD, Erwin E, Kayser A. Is the development of orientation selectivity instructed by activity? Journal of Neurobiology. 1999; 41:44–57. [PubMed: 10504191]

39. Anishchenko A, et al. Receptive field mosaics of retinal ganglion cells are established without visual experience. J Neurophysiol. 2010; 103:1856–1864. [PubMed: 20107116]

40. Jin JZ, et al. On and off domains of geniculate afferents in cat primary visual cortex. Nat Neurosci. 2008; 11:88–94. [PubMed: 18084287]

41. Jin J, Wang Y, Swadlow HA, Alonso JM. Population receptive fields of ON and OFF thalamic inputs to an orientation column in visual cortex. Nat Neurosci. 2011; 14:232–238. [PubMed: 21217765]

42. Tavazoie SF, Reid RC. Diverse receptive fields in the lateral geniculate nucleus during thalamocortical development. Nature Neuroscience. 2000; 3:608–616. [PubMed: 10816318]

43. Smith SL, Hausser M. Parallel processing of visual space by neighboring neurons in mouse visual cortex. Nat Neurosci. 2010; 13:1144–1149. [PubMed: 20711183]

44. Niell CM, Stryker MP. Highly selective receptive fields in mouse visual cortex. J Neurosci. 2008; 28:7520–7536. [PubMed: 18650330]

45. Vanduffel W, Tootell RBH, Schoups AA, Orban GA. The organization of orientation selectivity throughout macaque visual cortex. Cerebral Cortex. 2002; 12:647–662. [PubMed: 12003864]

46. Poggio GF, Baker FH, Mansfield RJ, Sillito A, Grigg P. Spatial and chromatic properties of neurons subserving foveal and parafoveal vision in rhesus monkey. Brain Res. 1975; 100:25–59. [PubMed: 810220]

47. Das A, Gilbert CD. Distortions of visuotopic map match orientation singularities in primary visual cortex. Nature. 1997; 387:594–598. [PubMed: 9177346]

48. Blasdel GG. Orientation Selectivity, Preference, and Continuity in Monkey Striate Cortex. Journal of Neuroscience. 1992; 12:3139–3161. [PubMed: 1322982]

49. Benucci A, Ringach DL, Carandini M. Coding of stimulus sequences by population responses in visual cortex. Nat Neurosci. 2009; 12:1317–1324. [PubMed: 19749748]

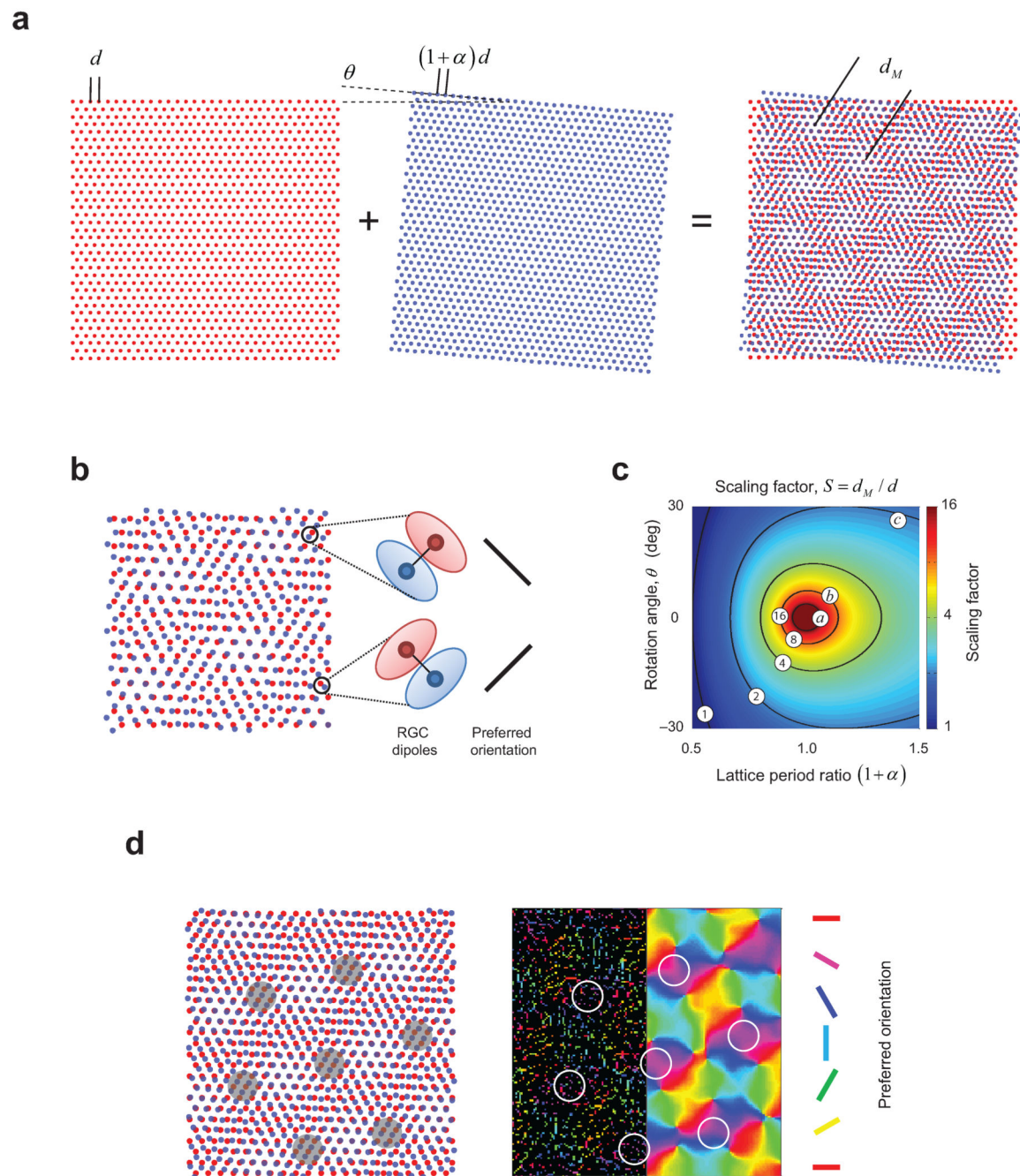50. Perona P. Orientation diffusions. IEEE Trans Image Process. 1998; 7:457–467. [PubMed: 18276265]

Figure 1.
Orientation maps as moiré interference pattern between retinal ganglion cell mosaics. **a.** Superposition of two hexagonal results in a periodic interference pattern. **b.** Locally, patterns are organized into pairs of dipoles, where cells of opposite center sign are nearest neighbors of each other. Cortical pooling of inputs from a dipole would result in simple-cell receptive fields with side-by-side ON/OFF sub-regions. **c.** The period of the interference pattern is a function of the ratio between the lattice spacing in the two mosaics and their relative orientation. The operating points *a, b* and *c*, lead to scaling factors of 21, 8.1 and 2.2

respectively, and these operating regimes are also used in the following figures. **d.** Example of an orientation map generated from a moiré interference pattern. The left panel shows the moiré interference pattern between ON and OFF center receptive fields. Shaded areas on the moiré interference pattern show that dipoles with the same orientation arrange themselves as vertices of a hexagonal lattice pattern (see also Fig 2c). In the right panel, which represents the same area shown by the pattern on the left, the resulting cortical orientation tuning is shown in two ways. The left half of the map shows the preferred orientation of well-tuned cortical cells (OSI>0.25) coded by their preferred orientation. The smooth map in the right half is obtained by Gaussian filtering of these strongly tuned orientation signals[50] (see **Methods** for details). Dipole orientation (left panel) determines the preferred orientation of the best tuned neurons in the cortex (right panel). Outlined white circles on the right panel correspond to the same iso-orientation domains depicted on the interference pattern on the left.
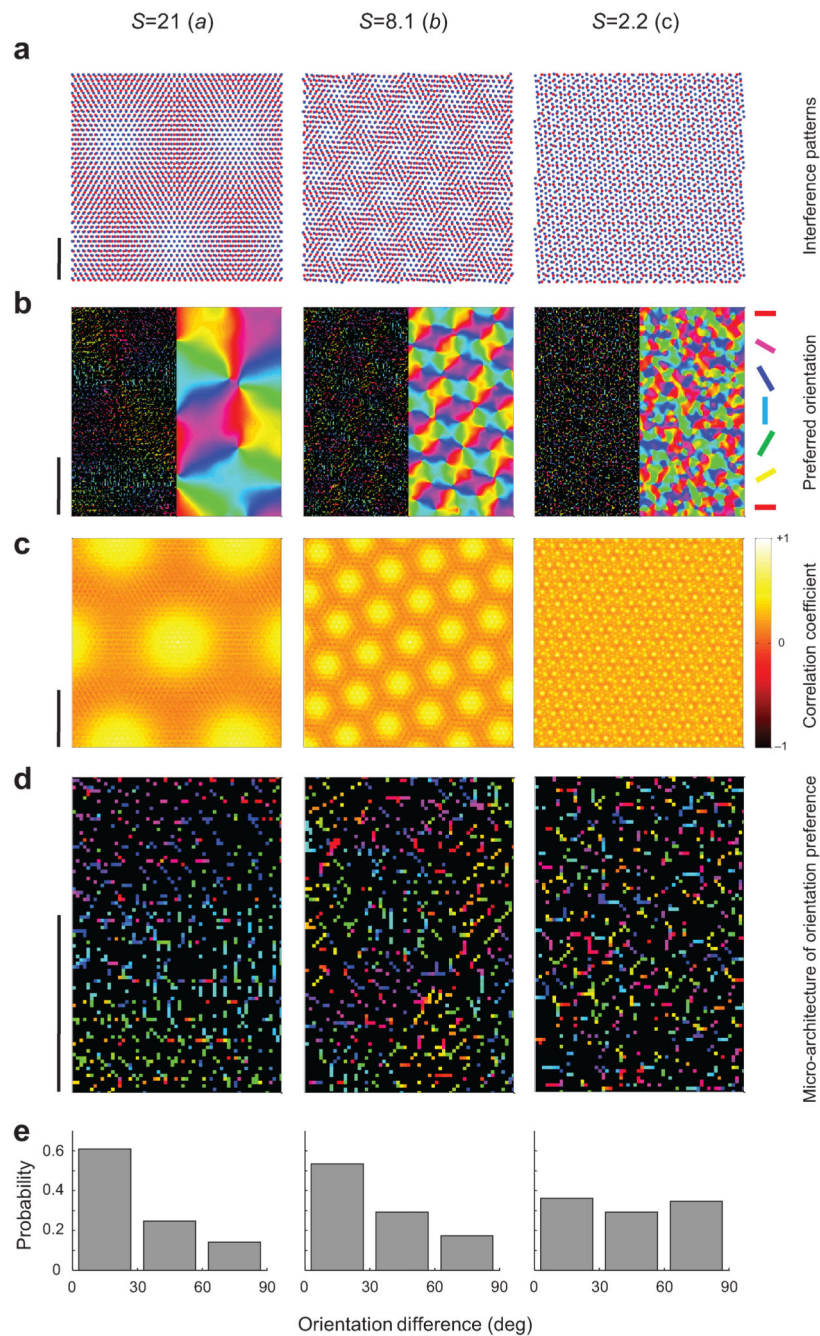
Figure 2.
Moiré scaling factor and orientation map periodicity. Each column depicts examples of different scaling factors. The operating regimes illustrated are the ones shown by *a, b*, and *c* in Fig 1c **a.** Examples of the resulting moiré interference patterns. Scale bar represents 1mm on the retinal surface. **b.** Preferred orientations of well tuned cells (Left) and filtered orientation map (Right). See legend in Fig 1d for an explanation of this format. **c.** Auto-correlations of orientation maps show hexagonal structure, indicating that iso-orientation domains lie on a hexagonal lattice (see also Fig. 1d). **d.** Enlarged area from the maps in **b**

showing the predicted micro-architecture of orientation preference. Preferred orientation changes gradually in the left and middle panels. In the right panel, orientations are distributed as a salt-and-pepper-like pattern. **e.** Histogram of the orientation differences between pairs of nearby cells (<100μm) on the cortical surface. Similar orientations cluster in the left and middle panels. In the right panel preferred orientations at nearby locations are uncorrelated. The uniform distribution of angular differences in the right histogram is a signature of salt-and-pepper organization. In **b–d** the scale bar represents 1mm of cortical space.
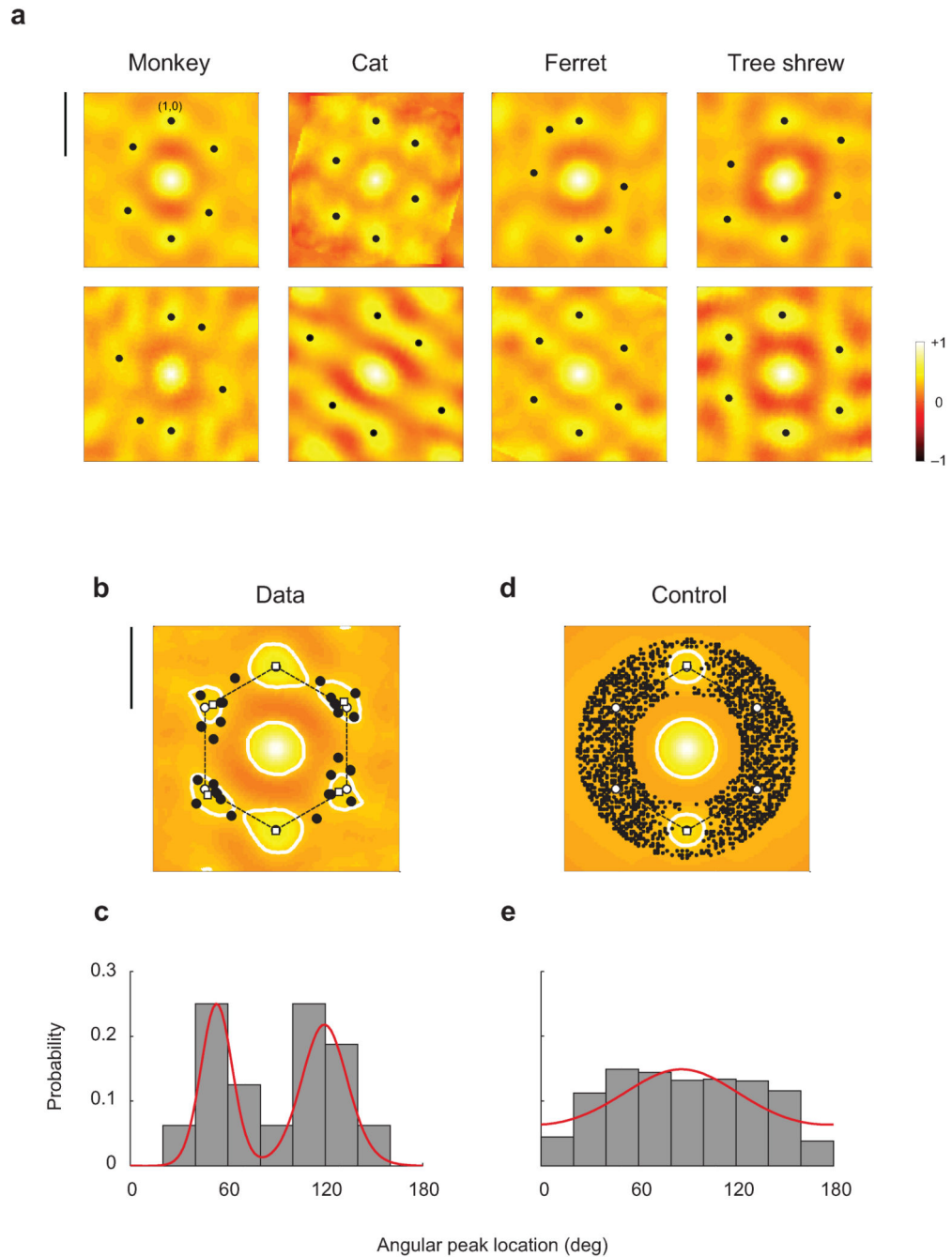
Figure 3.

Hexagonal structure of orientation maps. **a.** The autocorrelation structure of orientation maps are shown for two different animals in four species. Note that secondary peaks in the autocorrelation function form an approximate hexagonal structure in all cases. The magnitude of all these local maxima are statistically significant (Bootstrap analysis, $p < 0.002$) Scale bar equals the orientation map period. **b.** The average auto-correlation function across all animals shows local peaks (open squares) that match closely the ones predicted by a perfect hexagonal lattice (open circles). The solid dots represent the locations of all the

local maxima (shown in panel **a**) after the normalization step. Contour lines were plotted at a correlation coefficient level of 0.33 to illustrate the separation of local peaks. Scale bar equals the orientation map period. **c.** Angular location of local peaks in the auto-correlation function in panel **b.** The distribution is bimodal with modes near 60 and 120 degrees, as predicted by the model. Bimodality was established via a mixture of von Mises distributions using Bayes information criterion to select the order of the model. The red solid line shows the probability distribution of the best fit. **c,d.** Same analysis performed on control maps. Here the distribution of local peaks is much more isotropic. One component (red line) is sufficient to account for the control data. In **a–d** local peaks were considered only if their distances to the origin where within 33% of the map period.
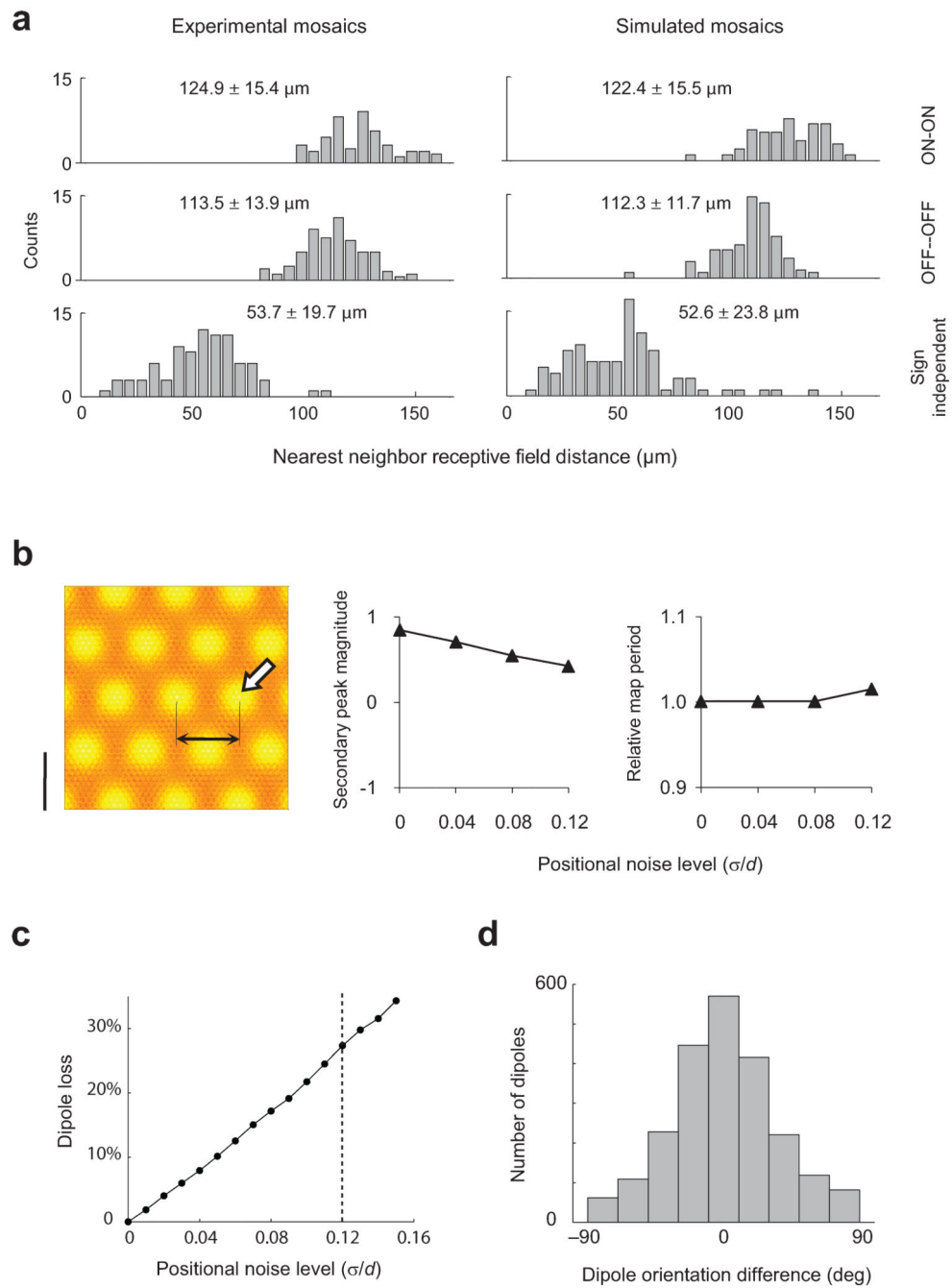
a

Experimental mosaics   Simulated mosaics

124.9 ± 15.4 µm   122.4 ± 15.5 µm   ON–ON

113.5 ± 13.9 µm   112.3 ± 11.7 µm   OFF–OFF

53.7 ± 19.7 µm   52.6 ± 23.8 µm   Sign independent

Counts

Nearest neighbor receptive field distance (µm)

b

Secondary peak magnitude

Relative map period

Positional noise level (σ/d)

c

Dipole loss

Positional noise level (σ/d)

d

Number of dipoles

Dipole orientation difference (deg)

Figure 4.

Robustness of seeded map to positional noise. **a**. The addition of independent Gaussian
noise of an appropriate magnitude to the positions of vertices in the hexagonal lattice
enables the model RGC mosaic to match the statistics of nearest neighbor distance
distributions observed experimentally, both within and across cell types. The experimental
data shows the distance between receptive field center locations. The standard deviation of
the Gaussian noise required to match these distributions equals $s = 0.12´ d$. **b.** The
periodicity and strength of the seeded structure can be measured by the distance from the

origin (black arrows) and magnitude of secondary peaks (white arrow) in the auto-correlation of the orientation map. As noise level increases up to realistic values the secondary peak in autocorrelation remains strong and the map period is invariant, showing the robustness of moiré interference pattern. The map period is plotted relative to that attained in the absence of positional noise. **c.** Percent of ON/OFF dipoles originally present in the noise-free interference pattern that are lost with increasing noise levels. The vertical line indicates the level required to match nearest neighbor distributions, $s = 0.12´ d$. For this noise level 27% of the dipoles are lost on average. **d.** Dipoles that survive the perturbation of their location will have their original orientation perturbed. The histogram shows the distribution of changes in orientation in a dipole from its original orientation at experimental noise levels, $s = 0.12´ d$.
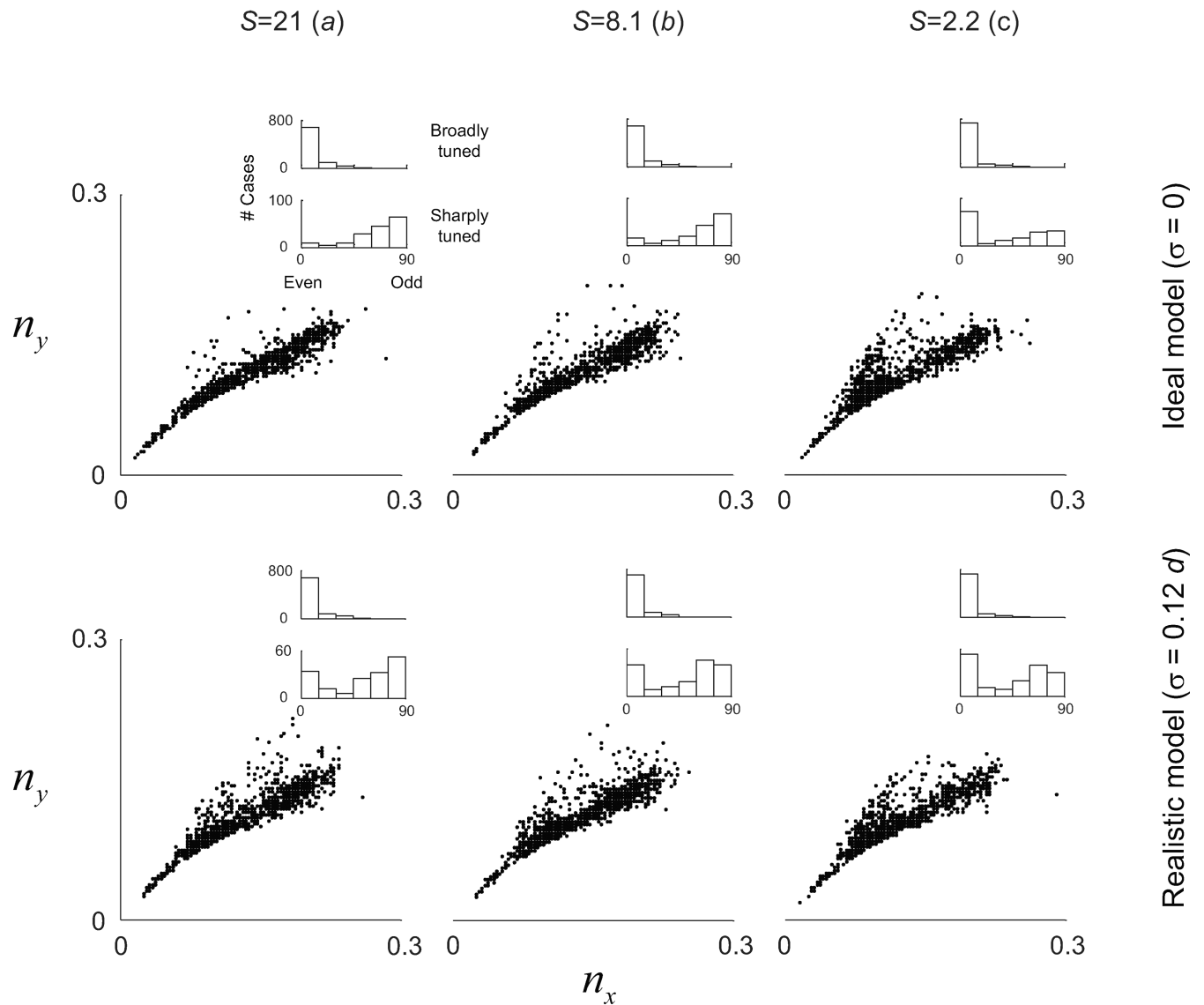
Figure 5.
Robustness of receptive field shapes at different operating regimes of the model. Receptive field structure was evaluated by the distribution of (n_x, n_y) and of spatial phases of the simulated receptive fields. The distributions are similar for the different operating regimes, despite the fact that some do not support the existence of smooth orientation maps. Insets show the distribution of spatial phases in broadly tuned (bottom 50%) and sharply tuned (top 10%) of simulated receptive fields.